Kinetic-energy dependence of competitive spin-allowed and spin-forbidden reactions: $V^+ + CS_2$

Chad Rue and P. B. Armentrout
Department of Chemistry, University of Utah, Salt Lake City, Utah 84112

Ilona Kretzschmar, Detlef Schröder, Jeremy N. Harvey, and Helmut Schwarz
Institut für Organische Chemie der Technischen Universität Berlin, Strasse des 17. Juni 135, D-10623 Berlin, Germany

(Received 4 December 1998; accepted 27 January 1999)

The kinetic-energy dependence of the $V^+ + CS_2$ reaction is examined using guided ion-beam mass spectrometry. Several different ion sources are used to systematically vary the V^+ electronic state distributions and elucidate the reactivities of both the ground and excited state V^+ cation. The cross section for VS^+ formation from ground state $V^+(^5D)$ exhibits two endothermic features corresponding to the formation of ground state $VS^+(^3\Sigma^-)$ and excited state $VS^+(^5\Pi)$. The thresholds for these two processes are in good agreement with theoretically determined excitation energies. The cross section for spin-forbidden formation of ground state $VS^+(^3\Sigma^-)$ exhibits an unusual variation with kinetic energy that is attributed to the energy dependence of the surface-crossing probability. From the thresholds associated with the formation of VS^+ and $V(CS)^+$, $D_0(V^+-S)=3.72\pm0.09$ eV and $D_0(V^+-CS)=1.70\pm0.08$ eV are derived. Further, circumstantial evidence for formation of a high-energy isomer of $V(CS)^+$ is obtained. © *1999 American Institute of Physics.* [S0021-9606(99)01116-2]

I. INTRODUCTION

The chemistry of transition metals and their compounds is strongly influenced by the availability of multiple low-lying electronic states in these species.[1,2] During the course of a chemical reaction, the ability of the metal center to access these states and adapt to different bonding situations may enable the system to find low-energy reaction pathways that would not be accessible otherwise. This type of nonadiabatic behavior, in which more than one electronic state determines the minimum energy pathway of a reaction, has been referred to as two-state reactivity (TSR).[3,4] Understanding the role of individual electronic states in chemical reactions is of obvious fundamental interest, but could also aid in the development and optimization of selective catalysts for industrial processes.

Gas-phase studies of state-specific reactions have the advantage that reactive encounters can be isolated and controlled with much greater precision than in condensed phases. The study of ion–molecule reactions is particularly facile, because mass spectrometric techniques can be used to isolate reactants and characterize products. Additionally, the kinetic energy of the ionic reactants is easily varied, which allows the experimentalist to probe energy regions where TSR can occur. Guided ion-beam (GIB) mass spectrometry has been used extensively to study the dynamics and thermochemistry of ion–molecule reactions, including examples of state-specific processes and TSR.[1,5,6]

In this paper, we present a particularly interesting system in which surface-crossing behavior is observed, i.e., C–S bond activation of carbon disulfide by atomic vanadium cation,

$$V^+ + CS_2 \rightarrow VS^+ + CS \quad (1)$$

$$\rightarrow [V,C,S]^+ + S. \quad (2)$$

The kinetic-energy dependence of these processes is studied over an extended range, and particular attention is paid to the role of the electronic states of the V^+ reactant. We find that reaction (1) exhibits both adiabatic and nonadiabatic behavior, and thus allows an investigation of the kinetic-energy dependence of a process involving TSR.

II. EXPERIMENT

A. Guided ion beam mass spectrometer

The kinetic-energy dependence of the $V^+ + CS_2$ reaction is studied using a guided ion beam mass spectrometer, which has been described in detail previously.[7,8] Briefly, V^+ ions are generated in one of several interchangeable ion sources, described below. Ions produced in the source are accelerated and passed through a magnetic sector for mass selection. The mass-selected V^+ beam is then decelerated to a desired kinetic energy and focused into a rf octopole,[9] which guides the ions through a static gas cell. Here, CS_2 is introduced at pressures between 0.05 and 0.1 mTorr such that V^+ ions typically encounter no more than one CS_2 molecule as they traverse the gas cell. The ionic products formed in the ensuing chemical reaction, as well as unreacted V^+ ions, drift to the end of the octopole where they are extracted and passed through a quadrupole mass filter for analysis. Ions are detected with a secondary electron scintillation ion detector using standard pulse counting techniques. The kinetic energy of the ions is varied during the experiment by adjusting the dc bias on the octopole rods with respect to the potential of

the ion-source region. Reactant and product ion intensities are measured at many different collision energies, both with and without CS_2 in the gas cell. As described previously,[7] lab-frame energies are converted to center-of-mass energies, and reaction cross sections are calculated from the product intensities relative to the reactant intensity after correcting for the background signal.

B. Data analysis

The kinetic-energy dependence of product cross sections is analyzed to determine E_0, the energy threshold for product formation at 0 K. E_0 differs from the apparent threshold observed under laboratory conditions due to the Maxwell–Boltzmann velocity distribution of the neutral gas molecules, the kinetic-energy distribution of the ion beam (which is nearly Gaussian), and the internal energy of the reactants. Each of these contributions allows the reaction to occur at energies below E_0. Experimental data are modeled with a variation of the line-of-centers model,

$$\sigma(E)=\sigma_0\Sigma g_i(E+E_{\rm int}+E_i-E_0)^n/E^m, \tag{3}$$

in which σ_0, E_0, and n are treated as adjustable parameters, E is the relative kinetic energy of the reactants, and $E_{\rm int}$ is the internal (rotational and vibrational) energy of CS_2 (0.047 eV at 300 K).[10] The summation is over the electronic states of V^+ having energies E_i and populations g_i, where $\Sigma g_i=1$. The parameter m is set equal to 1 except in unusual circumstances (see below).

An optimization routine is used in which incremental changes are made to the adjustable parameters in Eq. (3), which is then convoluted over the experimental energy distributions and compared to the data. The process is repeated until the convoluted form of Eq. (3) satisfactorily reproduces the experimental data. The uncertainty in E_0 values reflects both the uncertainty in the absolute laboratory energy scale (0.05 eV) and the distribution of threshold values obtained in the modeling procedure, as a range of fitting parameters yields satisfactory fits to the data.

At higher reaction energies, products may be formed with sufficient excess internal energy that they dissociate. In such a process, the decline of the product cross section due to dissociation may be modeled with a modified form of Eq. (3),

$$\sigma(E)=\sigma_0[\Sigma g_i(E+E_{\rm int}+E_i-E_0)^n/E^m][1-P_D(E-E_0)]. \tag{4}$$

The dissociation probability, P_D, incorporates statistical considerations involving angular momentum and cannot be given in simple form. For a detailed discussion, see Ref 11. In brief, P_D is controlled by three parameters: D, the bond dissociation energy of the ionic product which is fixed by the thermochemistry of the system, f, the fraction of the products' internal energy contained in the ionic species, and p, a parameter similar to n. During optimization, f and p are treated as adjustable parameters (although p is held to integral values).

C. Ion sources

In order to characterize the role of electronically excited V^+ in the CS_2 reactions, three different ion sources are used in this study to systematically vary the V^+ state distribution.

1. DC discharge/flow tube (DC/FT)

V^+ ions are created in a dc discharge plasma by Ar^+ sputtering of a negatively charged vanadium cathode. This source includes a flow tube immediately following the discharge region in which the ions undergo $\sim 10^5$ collisions with ~10% Ar in He buffer gas to cool the ions.[8] The total pressure in this region is typically 0.6–1 Torr. Because not all excited electronic states of V^+ are quenched by helium or argon collisions under these conditions,[12] we also add small amounts (1–5 mTorr) of CH_4 or NO to the flow tube to enhance quenching. Excited V^+ ions in the $a\,^3F$ and higher states react exothermically with CH_4 and NO at room temperature (predominantly to form VCH_2^+ and VO^+, respectively)[13] which effectively removes these ions from the reactant beam upon mass selection. This approach does not quench the $V^+(^5F)$ first excited state, which is unreactive with both gases at room temperature.[14] Although collisional quenching by Ar, CH_4, or NO may deactivate some of these excited ions, we assume that the ^5F state is present to some extent in our DC/FT V^+ beams (see below).

2. Surface ionization (SI)

In the surface ionization source, $VOCl_3$ vapor is exposed to a resistively heated rhenium filament. The compound decomposes on the filament, and V^+ ions desorb with a Maxwell–Boltzmann (MB) distribution of states characteristic of the filament temperature.[15] This temperature was previously calibrated as a function of the applied current by optical pyrometry assuming the filament acts as a blackbody radiator. Because the SI source does not utilize the flow tube, there is no collisional cooling, such that excited state ions produced by this source can only relax by emitting radiation. However, optical transitions between the low-lying states of V^+ are parity forbidden, because these states involve only s and d orbitals. Consequently, the lifetime of these states[16] almost certainly exceeds the flight time of the ions from the source to the reaction region (~1 ms). Therefore, we assume that the electronic state distribution of the V^+ reactant is the same as that produced by the source. Three different filament temperatures are examined: 1800, 2200, and 2300 K. The uncertainty in the absolute filament temperatures is estimated to be ±100 K, while the relative uncertainty is much lower. The V^+ state distribution calculated at these three temperatures is given in Table I.

3. Electron ionization (EI)

V^+ ions are also generated by electron ionization of VOC_3 at an electron energy of 30 eV. Previous studies of ions produced in this way have characterized the state distribution.[13,17,18] The results of this work are also given in Table I. As with SI, the EI source does not utilize the flow tube, and thus the state distribution of the V^+ reactant is expected to be the same as that produced by the ion source.

TABLE I. Approximate V^+ electronic state populations (%) produced by various ion sources.

State	Energy (eV)[a]	Electron config.	DC/FT (1250 K)[b,d]	DC/FT (1500 K)[c,d]	SI (1800 K)[d]	SI (2200 K)[d]	SI (2300 K)[d]	EI (30 eV)[e]
^5D	0.026	$3d^4$	94.15	90.55	86.11	80.56	79.27	40 (5)
^5F	0.363	$4s3d^3$	5.85	9.43	13.81	19.14	20.34	18 (9)
^3F	1.104	$4s3d^3$	0.004	0.018	0.070	0.230	0.290	7 (2)
Higher states			<0.001	0.002	0.013	0.075	0.107	35 (11)

[a]Energies are weighted averages (by degeneracies) over J levels, taken from Ref. 30.
[b]CH_4 added to flow tube as a chemical quenching agent. Temperature is estimated by comparison of exothermic feature to SI cross sections (see the text).
[c]No chemical quenching gases are used. Temperature is estimated by comparison of exothermic feature to SI cross sections (see the text).
[d]Maxwell–Boltzmann distribution at indicated temperature.
[e]Populations are from Refs. 12, 16, and 17.

D. Theoretical calculations

Density functional calculations are performed with Becke's three parameter hybrid method[19] using the correlation functional of Lee, Yang, and Parr (LYP)[20] and the 6-311+G* basis sets for vanadium, carbon, and sulfur as implemented in the GAUSSIAN94 program.[21] This method is referred to as *B3LYP*/6-311+G*. At this level of theory, the stationary points are characterized as minima or first-order transition structures by evaluating their vibrational frequencies and normal modes. Internal reaction coordinate calculations are used to further verify the relationship of minima and the associated transition structures. All calculated energies include zero-point energies.

The spin–orbit coupling constant (H_{SO}) of diatomic VS^+, used to estimate H_{SO} in the $[V,C,S_2]^+$ system (see below), is evaluated using the GAMESS program[22] together with a 6-31G* basis set for sulfur[23] and a triple-zeta basis set for vanadium.[24] These calculations apply an approximate one-electron operator with an effective nuclear charge (Z_{eff}) as an adjustable parameter to incorporate the missing two-electron terms.[25] A value of $Z_{eff}(S)=13.6$ has been recommended in the literature,[25] and $Z_{eff}(V)=10.5$ is chosen because it reproduces the experimental splitting in spin–orbit calculations on the $V^+(^5D)$ term. The spin–orbit coupling matrix elements between all substrates of the triplet and the quintet states of VS^+ are calculated using the complete active space self-consistent field (CASSCF) wave functions. The $^3\Sigma^-$ wave function is a fully optimized CASSCF wave function, with the active space including the molecular orbitals resulting from the $3d$ and $4s$ atomic orbitals of vanadium and the $3p$ atomic orbitals of sulfur. The $3s$ orbital of sulfur is not included, because this s-orbital mixes with the inner shell $3p_z$ orbital of vanadium.[26] The same approach is used for orbital optimization of the $^5\Pi$ wave function, except for the constraint that the 15 core orbitals are adopted from the triplet wave function.

III. RESULTS AND DISCUSSION

A. Excited states of the V^+ reactant

One possible probe for the presence of reactive excited states is to vary the ion source conditions and monitor changes in the cross sections of the products. In the present system, the cross section for formation of VS^+ in reaction (1) provides a convenient probe of electronically excited V^+ in the reactant beam. Figure 1 shows the cross sections obtained when V^+ is produced by EI, SI, and DC/FT sources. All of the cross sections exhibit a feature in the very low-energy region (<0.2 eV) corresponding to exothermic formation of VS^+ in reaction (1). The magnitude of this feature is strongly dependent on the ionization conditions. The SI cross sections are particularly informative, because the V^+ state distribution is well characterized (Table I). As illustrated in Fig. 1, the size of the exothermic feature increases with increasing filament temperature, unambiguously demonstrating that the low energy feature is due to the reaction of electronically excited V^+. The ratios of the magnitudes of the exothermic features (denoted as ratios of the filament temperatures) are 2300 K/1800 K = 4.7 ± 0.7, 2200 K/1800 K = 3.2 ± 0.7, and 2300 K/2200 K = 1.4 ± 0.2. These values are consistent with the calculated population ratios of the ^3F state in these experiments, 4.1, 3.3, and 1.3, respectively. Higher excited states may also contribute to the exothermic feature, but we are unable to determine their individual reactivities. Assuming that all of these states (^3F and above) are

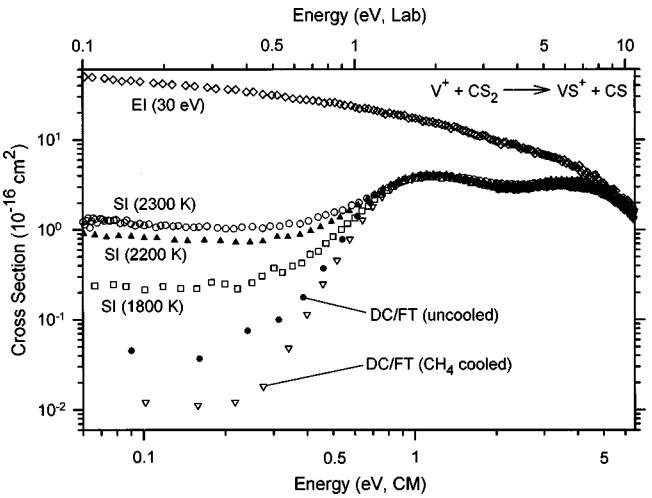

FIG. 1. Cross sections for VS^+ formation in reaction (1) as a function of kinetic energy in the center-of-mass (lower axis) and laboratory (upper axis) frames. Results are shown for V^+ ions formed by electron ionization (EI) at 30 eV (◇), surface ionization (SI) at 2300 K (○), 2200 K (▲), and 1800 K (□), and the dc discharge/flow tube (DC/FT) ion source both with (▽) and without (●) methane cooling in the flow tube.

equally reactive, the predicted exothermic feature ratios are 4.8, 3.7, and 1.3, respectively. These values are consistent with the observed ratios within experimental uncertainty. In contrast, the calculated ratios for states above the ^3F state are 8.2, 5.8, and 1.4, respectively. Similarly, the ratio of the ^5D and ^5F states cannot account for the experimental findings. This demonstrates that the ^3F state dominates the reactivity in the low energy region (<0.2 eV). Further, the good agreement between the experimentally observed exothermic cross-section ratios and the predicted population ratios of the ^3F (and possibly higher states) helps confirm the accuracy of both the SI filament temperatures and the assumption of a Maxwell–Boltzmann distribution of states.

The size of the exothermic feature obtained for ions produced by EI is much larger than that obtained by SI or DC/FT sources, consistent with previous studies which determined that EI produces a large fraction of excited V^+ (Table I).[13,17,18] The observed EI/SI exothermic cross-section ratios are EI/SI(2300 K)=37±3, EI/SI(2200 K)=54±7, and EI/SI(1800 K)=175±35. If only the ^3F state is considered, the information given in Table I predicts ratios of 24, 30, and 100, which are systematically lower than our experimental observations. This indicates the involvement of higher-lying reactive states. The predicted population ratios for all of the higher excited states (^3F and above) are 106, 138, and 506, respectively, i.e., much larger than the observed ratios. We therefore conclude that most of the exothermic feature in the EI experiment (60±10%) is due to the reaction of the ^3F state, but that higher lying states also contribute. Because the ^3F state comprises only 7±2% of the EI beam compared to 35±11% for the higher states, the ^3F state must be substantially more reactive toward CS_2 to form VS^+ than the other states reacting exothermically. This comparison highlights an important aspect in the analysis of systems with multiple electronic states of the reactant. Namely, cross sections are dependent on both the abundance and the reactivity of the contributing states, and reactivity need not monotonically increase with excitation energy.[1,27,28]

Although the actual electronic temperature of the DC/FT beam is unknown, the small size of the exothermic feature obtained with this source (Fig. 1) indicates that it is the coldest source used in this study. The exothermic feature can be further reduced by adding 1–5 mTorr of CH_4 or NO to the flow tube, as described above. The cooling effect is clearly illustrated in Fig. 1, and further corroborates our finding that the exothermic feature is due to the reaction of electronically excited V^+. Higher pressures have no further cooling effect, indicating that some of the excited states are not collisionally or chemically deactivated under our experimental conditions.[29]

By comparing the magnitudes of the exothermic features in the DC/FT experiments to those obtained by SI, we estimate the electronic temperature of the uncooled (no CH_4 or NO) DC/FTV^+ beam to be 1500±100 K. After cooling with methane, the ratios of the exothermic features suggest an electronic temperature of the V^+ reactant in the range 1200–1300 K. Clearly, these temperatures are only a first approximation to the actual electronic state distributions produced by the DC/FT source. The efficiencies of chemical and collisional quenching in the flow tube probably differ for the various excited states, and the state distribution of the V^+ ions as they exit the flow tube may not be Maxwellian. Nevertheless, as a first approximation, we estimate that the cooled DC/FT V^+ beam used in this study is characterized by an electronic temperature of 1250±100 K (Table I). This is consistent with the electronic temperatures estimated for other transition metal ions produced with the DC/FT ion source.[30]

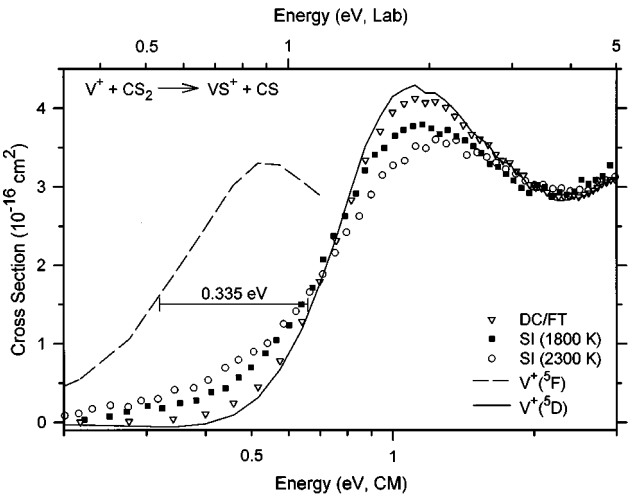

FIG. 2. Quintet cross sections for VS^+ formation as a function of kinetic energy in the center-of-mass (lower axis) and laboratory (upper axis) frames measured with surface ionization (SI) at 2300 K (○) and 1800 K (■) and methane cooled dc discharge/flow tube (DC/FT) (▽) ion sources. Extrapolated state-specific cross sections for the $V^+(^5D)$ state (the solid line) and the $V^+(^5F)$ state (the broken line) are also shown (see the text). The average energy splitting between these atomic states is also indicated.

B. Reactivity of $V^+(^5F)$ toward CS_2

The two endothermic features in the DC/FT and SI data (Fig. 1) are largely unaffected by the ion-source conditions. On the basis of the populations listed in Table I, these features must correspond primarily to the reaction of ground state $V^+(^5D)$, but the $V^+(^5F)$ first excited state may also contribute. Because the energies of these two states differ by only 0.335±0.001 eV,[31,32] the contributions of the ^5D and ^5F states are not easily resolved in GIB experiments. If reactive, the ^5F state is expected to appear in the VS^+ cross section as a shoulder on the low-energy side of the larger ^5D ground state feature. Our ability to observe reactions of this state is further masked by overlap from the exothermic channels, which obscures the rise of the cross section at low energies.

To explore the reactivity of the ^5F state, we assume that the shape of the EI cross section (which is due largely to states that react exothermically) is a good approximation to the energy dependence of the exothermic features in the SI and DC/FT cross sections. By appropriate scaling of the EI cross section, the exothermic reactivity can be subtracted from the SI and DC/FT data to approximate the individual endothermic ^5F and ^5D cross sections. The cross sections obtained by this method are subsequently referred to as quintet cross sections and are shown in Fig. 2. Note that the

threshold appears to shift to lower energies as the SI filament temperature is increased, consistent with the presence of a reactive, low-lying excited state. Additionally, the magnitude of the peak near 1 eV declines slightly with increasing temperature, reflecting the smaller population in the ^5D ground state at higher SI filament temperatures.

More detailed insight is obtained by modeling the data. By definition, the 0 K cross section depends only on the nature of the reactants. Consequently, the adjustable parameters σ_0, n, and E_0 in Eq. (3) should not be affected by the ion–source conditions, and the summation over electronic states together with the convolution over reactant kinetic-energy distributions should account for all variations in different data sets. When the quintet VS^+ cross sections are modeled assuming that the ^5F state is unreactive (that is, the sum over states includes only the spin–orbit levels of the ^5D ground state), we observe significant variations in the adjustable parameters σ_0, n, and E_0 as a function of the V^+ beam temperature (Table II). Therefore, the assumption that the ^5F state is unreactive toward CS_2 appears to be incorrect, and consequently, the modeling must explicitly include the ^5F state.

Clearly, the fitting parameters σ_0, n, and E_0 which describe the reaction cross section for the ^5F state need not be the same as those which describe the ^5D state. Nevertheless, as a first approximation, we assume that the n values for the two states are identical. In the absence of specific information to the contrary, this is the most reasonable starting assumption. The difference in the E_0 values for the various spin–orbit levels of both states is taken to be the known energy differences between these levels.[31] As the energy dependence of the two states is adequately described by Eq. (3), the remaining parameter, σ_0, determines the magnitude of a cross section and is therefore an energy-independent measure of the overall reactivity. Clearly, the σ_0 values for the ^5F and ^5D states may differ due to intrinsic differences in their reactivities. We therefore allow state-specific σ_0 values which reflect the relative reactivities of the ^5F and ^5D states. Among the wide range of $\sigma_0(^5F)/\sigma_0(^5D)$ reactivity ratios tested, the experimental data can be reproduced well with values from 0.5 to 1.0. The average values of σ_0, n, and E_0 for the ^5D ground state obtained at $\sigma_0(^5F)/\sigma_0(^5D)=0.5$ and 1.0 are given in Table II. Though a slight trend remains, these parameters exhibit much greater internal consistency than those obtained by neglecting the ^5F state. This result suggests that the overall reactivity of the $V^+(^5F)$ state toward CS_2 is $75\pm25\%$ compared to the $V^+(^5D)$ ground state.

Hence, the quintet cross sections shown in Fig. 2 can be regarded as linear combinations of the ^5D and ^5F state-specific cross sections, weighted according to the populations given in Table I and their relative reactivities as given by $\sigma_0(^5F)/\sigma_0(^5D)$. From the state populations in Table I, we can obtain a reasonable estimate of the ^5D and ^5F state-specific cross sections by extrapolating the quintet cross sections to ^5F populations of 0.0 and 1.0, respectively. These extrapolated state-specific cross sections are shown as lines in Fig. 2. Above about 0.7 eV, the experimental quintet cross section is dominated by the ^5D state, and the extrapolation is expected to be more accurate for the ^5D than for the ^5F state.

TABLE II. Fitting parameters for the first endothermic feature[a] of the quintet VS^+ cross sections.

Ion source	V^+ (^5F)	σ_0	E_0	n
DC/FT (cooled)	Neglected	10.4 (3.4)	0.63(0.02)	1.1 (0.2)
SI (1800 K)		8.1 (0.7)	0.30(0.09)	2.6 (0.6)
SI (2200 K)		7.9 (0.5)	0.37(0.07)	2.0 (0.5)
SI (2300 K)		6.7 (0.4)	0.45(0.08)	1.5 (0.4)
DC/FT (cooled)	Included[b]	7.9 (1.5)	0.73(0.04)	0.58 (0.13)
SI (1800 K)		6.6 (0.4)	0.75(0.04)	0.51 (0.07)
SI (2200 K)		6.5 (0.2)	0.78(0.05)	0.45 (0.07)
SI (2300 K)		5.9 (0.4)	0.80(0.04)	0.42 (0.05)
Extrapolated V^+ (^5D)		7.5 (0.4)	0.76(0.02)	0.46 (0.08)
Extrapolated V^+ (^5F)		3.7 (0.8)	0.41(0.02)	0.41 (0.18)

[a]Fits do not reproduce the decline of the first feature above 1 eV.
[b]Parameters are averages from fits at $^5F/^5D$ reactivity ratios of 0.5 to 1.0.

Moreover, small errors in the original data in this energy region are magnified in the extrapolation of the ^5F cross section, and hence this treatment is not extended above 0.7 eV. Below 0.7 eV, the quintet cross sections have appreciable contributions from the reaction of the ^5F state, and reasonable results are obtained. An analysis of these state-specific cross sections with Eq. (3) ($m=1$) yields $\sigma_0=7.5\pm0.4$, $E_0=0.76\pm0.02$ eV, and $n=0.46\pm0.08$ for $V^+(^5D)$ and $\sigma_0=3.7\pm0.8$, $E_0=0.41\pm0.02$ eV, and $n=0.41\pm0.18$ for $V^+(^5F)$. The threshold difference of 0.35 ± 0.03 eV is in good agreement with the average state separation of 0.33 ± 0.01 eV.[31] Further, the ratio of the σ_0 values, 0.49 ± 0.14, is consistent with the $\sigma_0(^5F)/\sigma_0(^5D)$ reactivity ratio of 0.75 ± 0.25 determined above. Finally, the fitting parameters for the extrapolated ^5D cross section are comparable to those in the lower half of Table II.

The relative reactivity of the ^5F and ^5D states determined here is consistent with that measured in elegant state-specific studies by Sanders, Hanton, and Weisshaar.[33] They used resonant two-photon ionization (R2PI) to produce vanadium ion beams of different electronic states and examined the reactivity with ethene, ethane, and propane. Although the reactivity of the quintet states is too small to be measured in the ethene and ethane systems, the $\sigma_0(^5F)/\sigma_0(^5D)$ reactivity ratio in the propane system at thermal energies is 0.4 ± 0.5. However, the observations that $V^+(^5F)$ reacts with CS_2 and propane contrast somewhat with previous findings that the ^5F state is relatively unreactive with H_2 and CH_4.[18] This may still be true, although it is also possible that these earlier studies were not particularly sensitive toward the ^5F state. In this regard, it should be noted that the sharply rising cross section observed for reaction (1) is ideal for observing differences in the reactivity of the closely spaced ^5D and ^5F states. Although these various studies do not yield a uniform relative reactivity difference between these states, they all agree that the ^5F is less reactive than the ^5D state. This result has been attributed to the high-spin $4s^13d^3$ electron configuration of $V^+(^5F)$, in which the $4s$ electron leads to a largely repulsive interaction with closed-shell molecules and reduces the probability of reactive collisions. In contrast, the $3d^4$ electron configuration of $V^+(^5D)$ ground state allows for a closer approach of the

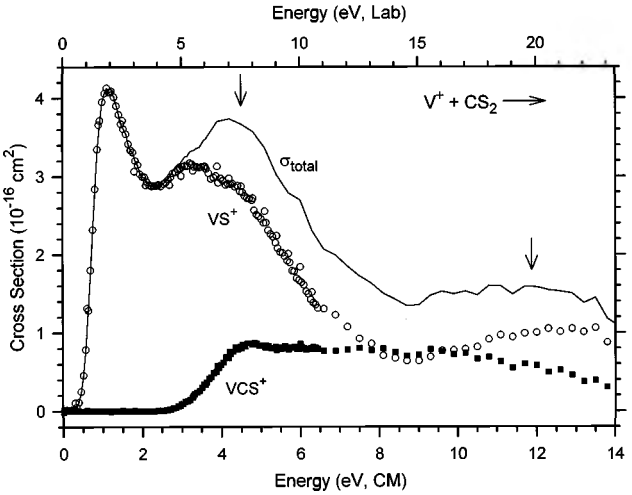

FIG. 3. Product cross sections for formation of VS^+ (○) and $[V,C,S]^+$ (■) as a function of kinetic energy in the center-of-mass (lower axis) and laboratory (upper axis) frames. Arrows mark the onsets of the dissociation reactions (7) and (10) at 4.50 and 11.87 eV, respectively.

reactants and thus is able to more efficiently activate bonds.[18] It is possible that the significant reactivity of $V^+(^5F)$ observed in this and Weisshaar's study may be due to the high polarizabilities[34] of CS_2 (8.74 Å^3) and C_3H_8 (6.29 Å^3) vs H_2 (0.79 Å^3) and CH_4 (2.60 Å^3), which leads to stronger ion-induced dipole interactions. It is also possible that the repulsive interactions arising from the occupied $4s$ electron of the $V^+(^5F)$ states are less severe with highly polarizable molecules like CS_2, in which the electron cloud is more easily distorted.

C. Assignment of cross-section features

The cooled DC/FT source generates a nearly pure ground state V^+ beam (Table I), and results for reaction (1) differ little from the extrapolated $V^+(^5D)$ cross section (Fig. 2). Hence, our subsequent discussion of reactions (1) and (2) refers to the experiments with the cooled DC/FT source. The cross sections for reactions (1) and (2) are plotted over an extended energy range in Fig. 3. VC^+, VS_2^+, and CS_2^+ products are also observed in minor quantities ($\sigma_{max}<0.02$ Å^2) as high-energy products (thresholds above 3 eV), but are omitted for clarity. The most interesting aspect is the presence of multiple endothermic features in the cross section of reaction (1), each suggesting a distinct mode of product formation. A complete understanding of this reaction requires both a qualitative assignment of these various features to specific processes (discussed in this section) and a quantitative description of their energy dependencies (see below).

The first endothermic feature in the VS^+ cross section corresponds to the formation of ground state VS^+ in reaction (1). This process has an apparent threshold near 0.4 eV, peaks around 1.2 eV, and falls to approximately two-thirds of its maximum intensity before the rise of a second endothermic feature near 2.3 eV. Because no products other than $VS^+ + CS$ are feasible in this energy range,[26] the second feature must correspond to the formation of electronically excited products. The energy difference between the two features is inconsistent with excitation of the CS neutral product, which requires 4.8 eV.[35] Therefore, the second process is assigned to the formation of electronically excited VS^+, and the energy difference between the two features provides a measure of the adiabatic excitation energy between two electronic states of VS^+.

The kinetic-energy dependence observed in the low-energy part of the VS^+ cross section is unusual. Although it is energetically possible to form excited product states in most ion–molecule reactions at elevated kinetic energies, individual product states rarely give rise to distinct features in GIB experiments. Clearly, the routes to the two products in question must differ in some fundamental way. Recent *ab initio* calculations[26] predict a $^3\Sigma^-$ ground state for VS^+ cation with the first quintet state ($^5\Pi$) lying 1.37 eV higher in energy. Thus, the formation of ground state products from ground state reactants in reaction (5) is spin forbidden, while at higher energies the spin-allowed reaction (6) can occur,

$$V^+(^5D) + CS_2(^1\Sigma_g^+) \rightarrow VS^+(^3\Sigma^-) + CS(^1\Sigma^+) \quad (5)$$

$$\rightarrow VS^+(^5\Pi) + CS(^1\Sigma^+). \quad (6)$$

The calculated energy difference between the $VS^+(^3\Sigma^-)$ and $VS^+(^5\Pi)$ states is in good agreement with the observed threshold difference between the two features in the VS^+ cross section (Fig. 3), and we therefore assign these features to reactions (5) and (6), respectively. The distinct fall and secondary rise of the cross section may therefore be regarded as a consequence of the spin-forbidden character of reaction (5), which leads to the decline above 1.2 eV (see below), combined with an enhanced reaction efficiency once the spin-allowed process (6) is energetically accessible.

Beginning at around 2.8 eV, the $[V,C,S]^+$ product begins to form in reaction (2), and a portion of the total reactivity shifts to this new channel. Chemical intuition implies that the $[V,C,S]^+$ product corresponds to a thiocarbonyl complex $V(CS)^+$ rather than an insertion species CVS^+ (see below). The onset of reaction (2) leads to a decrease in the VS^+ cross section near 3 eV, while the total cross section continues to increase monotonically. The observation that the $VS^+ + CS$ and $[V,C,S]^+ + S$ product channels compete directly suggests that these products evolve from a common intermediate, most likely the S–V^+–CS insertion species. If we consider the reverse reaction and combine the VS^+ and CS products along the lowest energy pathway, it seems clear that CS will approach the vanadium end of the VS^+ diatom and, likewise, that the S atom will prefer binding to the vanadium end of the $V(CS)^+$ triatom. Further, the potential-energy surface for the analogous reaction of V^+ with CO_2 includes the bond insertion intermediate, O–V^+–CO, a species that could also be probed by independent experimental means.[36] The conjecture of a S–V^+–CS intermediate does not preclude the possibility that more direct pathways for forming VS^+ and $V(CS)^+$ also contribute to the observed cross sections.

As the kinetic energy of the reaction is increased further, the VS^+ and $[V,C,S]^+$ products may be formed with sufficient excess internal energy that they dissociate in the overall

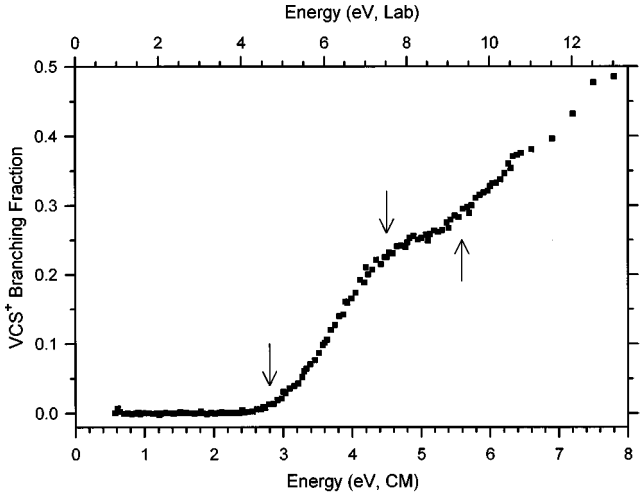

FIG. 4. Branching fraction of the $[V,C,S]^+$ product as a function of kinetic energy in the center-of-mass (lower axis) and laboratory (upper axis) frames. Arrows mark the onsets of reactions (2), (7), and (8) at 2.80, 4.50, and 5.60 eV, respectively.

reaction (7), which is energetically equivalent to simple cleavage of the S–CS bond ($D_0 = 4.50$ eV),[26]

$$V^+ + CS_2 \rightarrow V^+ + S + CS. \quad (7)$$

Once accessible, this dissociation channel decreases the probability of forming stable product ions in reactions (1) and (2), which leads to a decrease in both cross sections above 4.50 eV.

Interestingly, the $[V,C,S]^+$ cross section declines only slightly and levels out near 5.6 eV. This behavior is more clearly visible by plotting the branching fraction, $\sigma(VCS^+)/\sigma(\text{total})$, shown in Fig. 4. Note that the fraction of $[V,C,S]^+$ increases initially from its threshold, begins to slow at 4.5 eV due to dissociation, and then starts to increase more rapidly again near 5.6 eV. This second rise can conceivably be attributed to an isomer or excited state of $[V,C,S]^+$ or an excited state of S (see below). One possibility is

$$V^+ + CS_2 \rightarrow CVS^+ + S, \quad (8)$$

in which the ionic product has both the C and S atoms bound directly to the metal. This latter species could be formed from a $SV(CS)^+$ intermediate by cleavage of the C–S bond.

The VS^+ cross section exhibits a third endothermic feature beginning near 8 eV (Fig. 3), consistent with the expected threshold[26] for reaction (9),

$$V^+ + CS_2 \rightarrow VS^+ + C + S, \quad (9)$$

7.37 ± 0.04 eV above the onset for reaction (1), i.e., at about 8.2 eV. Reaction (9) is plausibly attributed to simple decomposition of a CVS^+ species by cleaving the V–C bond. This would explain why the onset of reaction (9) coincides with a slight decrease in the $[V,C,S]^+$ cross section above 9.5 eV.

Finally, the observed decrease in the total cross sections above 12 eV is attributed to complete atomization of CS_2 according to

$$V^+ + CS_2 \rightarrow V^+ + C + 2S. \quad (10)$$

The associated thermodynamic threshold of 11.87 ± 0.06 eV is in good agreement with the experimental result.

D. Surface-crossing behavior

As described above, competition and successive dissociations provide a complete description of the $[V,C,S]^+$ channel and the second and third features of the VS^+ cross section. Yet, neither dissociation nor competition can account for the early decline of the first feature in the VS^+ cross section. We believe this unusual kinetic-energy dependence can be explained by considering the effect of the surface-crossing probability on the spin-forbidden reaction (5). In the discussion that follows, the term adiabatic refers to an event in which the reaction remains on a single potential-energy surface as it evolves from reactants to products. In this regard, an adiabatic surface is defined by consideration of the full Hamiltonian including spin-orbit coupling terms. For the V^+/CS_2 system, the lowest-energy adiabatic surface is quintetlike in the reactant region, $V^+(^5D) + CS_2(^1\Sigma^+)$, and tripletlike in the product region, $VS^+(^3\Sigma^-) + CS(^1\Sigma^+)$, and thus involves a spin inversion. The term diabatic refers to an event in which the system retains its original spin, thereby crossing between adiabatic potential-energy surfaces at an avoided crossing. This type of diabatic behavior is referred to as single-state reactivity (SSR), while the adiabatic behavior is two-state reactivity (TSR).[3] A crucial aspect in the competition of SSR and TSR is that spin inversion *via* the adiabatic pathway often allows access to energetically favorable reaction pathways, while spin conservation in the diabatic pathway is entropically preferred once it is energetically feasible.

The formation of VS^+ at the thermochemical threshold for reaction (5) is an example of TSR because it requires spin inversion en route from the $V^+(^5D) + CS_2(^1\Sigma^+)$ reactants to the $VS^+(^3\Sigma^-) + CS(^1\Sigma^+)$ products. Therefore, the shape of the first feature in the VS^+ cross section should depend on the behavior of the reaction at the crossing between the diabatic quintet and triplet surfaces. At low kinetic energies, the reactants pass slowly through the crossing region, allowing the electrons to adjust to different configurations along the reaction coordinate. Under such conditions, spin inversion can be efficient, and adiabatic behavior is expected. As the nuclear motion speeds up at elevated energies, the reactants pass more quickly through the crossing region, the electrons have less time to adapt, and the Born–Oppenheimer approximation begins to fail. Thus, as the kinetic energy of the reactants increases, it becomes increasingly likely that the reactants will behave diabatically during the collision event. This increased probability for crossings between adiabatic surfaces (i.e., spin conservation) at higher kinetic energies appears to be responsible for the premature decline of the first feature associated with the formally spin-forbidden reaction (5). Thus, the VS^+ cross section decreases from the maximum near 1.2 eV until formation of the excited quintet state $VS^+(^5\Pi)$ is energetically feasible near 2 eV.

In order to get more detailed insight into the potential-energy surface of the $[V,C,S_2]^+$ system, density functional theory is used to calculate the reactant and product complexes, $V(CS_2)^+$ and $SV(CS)^+$, as well as the related transition structures (TSs) on the triplet and quintet surfaces (Fig. 5). The geometries and relative energies are given in Table

TABLE III. Calculated geometries [Å and deg] and relative energies [eV] for the $[V,C,S_2]^+$ system. Values in parentheses are derived from calculations at a higher level of theory; for details see Ref. 25.

Species	r_{V-S_1}	r_{V-C}	r_{S_1-C}	r_{C-S_2}	$\angle S_1-V-C$	$\angle V-C-S_2$	Energy[a]
$V^+(^5D)+CS_2(^1\Sigma^+)$			1.56	1.56			0.00[0.00]
$V^+(^3P)+CS_2(^1\Sigma^+)$			1.56	1.56			1.33[1.40]
$V(CS_2)^+$, $\mathbf{1}(^5A'')$	2.35	2.22	1.64	1.57	42	125	−1.17
$V(CS_2)^+$, $\mathbf{1}(^3A'')$	2.27	2.12	1.70	1.59	45	144	−0.67
TS $\mathbf{1/2}(^5A'')$	2.25	2.01	2.49	1.53	71	180	0.07
TS $\mathbf{1/2}(^3A'')$	2.12	1.99	1.92	1.56	56	161	−0.63
$SV(CS)^+$, $\mathbf{2}(^5A'')$	2.26	2.04	3.38	1.52	104	176	−0.04
$SV(CS)^+$, $\mathbf{2}(^3A'')$	2.03	2.04	2.93	1.52	92	180	−1.06
$VS^+(^5\Pi)+CS(^1\Sigma^+)$	2.23			1.54			2.28(2.03)[2.23]
$VS^+(^3\Sigma^-)+CS(^1\Sigma^+)$	2.02			1.54			1.22(0.66)[0.78]

[a]Values calculated at the B3LYP/6-311+G* level of theory. Experimental values are in brackets. Values in parentheses are derived from calculations at a higher level of theory; for details see Ref. 25.

III. As expected, the $V(CS_2)^+$ encounter complex **1** has a $^5A''$ ground state correlating with $V^+(^5D)+CS_2$ ground state reactants. However, coordination of carbon disulfide to vanadium significantly lowers the triplet surface compared to atomic V^+, and $\mathbf{1}(^3A'')$ is predicted to be 0.67 eV below the $V^+(^5D)+CS_2$ entrance channel. Except for the shorter V–S bond length (r_{V-S}) in the triplet, the calculated structures of $\mathbf{1}(^5A'')$ and $\mathbf{1}(^3A'')$ are quite similar (Table III). The same conclusion can be drawn for the $SV(CS)^+$ product complexes, $\mathbf{2}(^3A'')$ and $\mathbf{2}(^5A'')$, which have almost identical bond lengths and angles except for r^+_{V-S}, 2.03 Å in the triplet state compared to 2.26 Å in the quintet state. However, the order of stability is reversed for $SV(CS)^+$ in that the ground state is $^3A''$. These differences simply reflect the relative stability of the respective fragmentation channels, i.e., the ^5D ground state of atomic V^+ correlates to the $V(CS_2)^+(^5A'')$ reactant complex and the $^3\Sigma^-$ ground state of the VS^+ fragment leads to the $^3A''$ ground state of $SV(CS)^+$. Note that the B3LYP calculations overestimate the endothermicity of reaction (1) by about 0.5 eV. This effect can largely be ascribed to limitations in the description of the fragments with B3LYP, and is assumed to be negligible with regard to the relative energetics of **1** and **2**. Thus, the theoretical results indicate the occurrence of TSR as the lowest-energy pathway for bond activation of CS_2 by vanadium cation. In complete agreement with the conceptual implications of the TSR model, the barrier for bond activation is calculated to be significant on the high-spin, quintet surface, but small for the low-spin complex, i.e., TS$\mathbf{1/2}(^5A'')$ is ~1 eV above $\mathbf{1}(^5A'')$ while TS$\mathbf{1/2}(^3A'')$ is only 0.04 eV above $\mathbf{1}(^3A'')$. Because the order of stabilities is the opposite for the product complexes **2**, the barriers for the reverse processes are low for the quintet, but high for the triplet species. In fact, within the estimated uncertainty of the computational method, the global minimum of the $[V,C,S_2]^+$ system could be either $\mathbf{1}(^5A'')$ or $\mathbf{2}(^3A'')$.

Inspection of Fig. 5 allows us to estimate the position of the minimum energy crossing point (MECP) between the quintet and triplet surfaces.[37,38] We have not attempted to explicitly locate the MECP by theory, because it is expected to be situated between the closely spaced $\mathbf{1}(^3A'')$ and TS $\mathbf{1/2}(^3A'')$ species. Therefore, we estimate that the MECP lies at -0.6 ± 0.1 eV relative to the $V^+(^5D)+CS_2$ entrance channel. A crude estimate for the spin–orbit coupling constant (H_{SO}) at the MECP geometry can be gained by further *ab initio* calculations which explicitly treat the different spin–

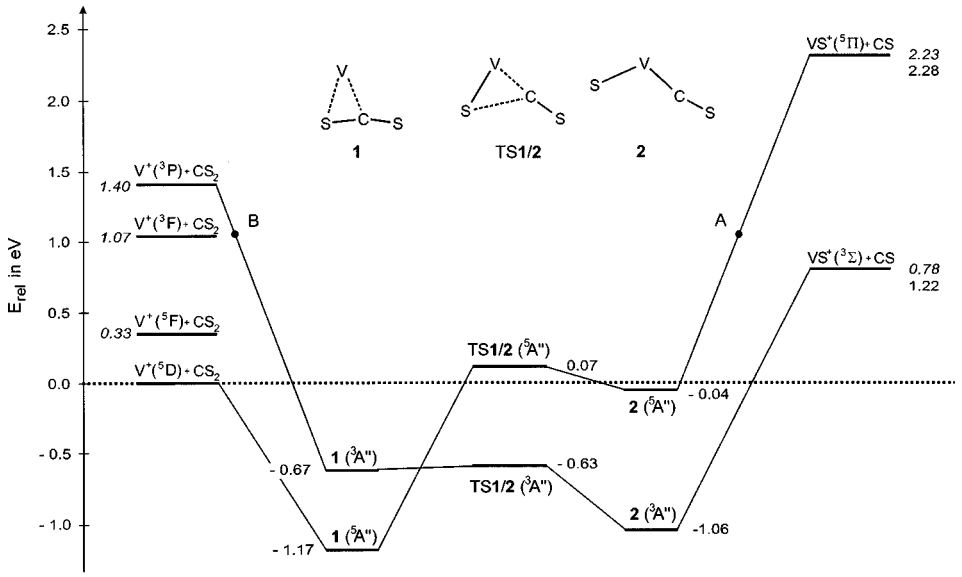

FIG. 5. Potential-energy curves for the $[V,C,S_2]^+$ system calculated at the B3LYP/6-311+G* level of theory. Experimental energies for the reactant and product asymptotes are given in italics.

orbit states (see computational details). It is expected that the main contribution to spin–orbit coupling (SOC) comes from the heavy atoms involved. Therefore, it appears a reasonable compromise to approximate the coupling constant for the triplet and quintet species at the MECP by calculating the SOC between triplet and quintet VS^+ at $r_{V-S}=2.12$ Å, i.e., taking the average of r_{V-S} in the triplet and quintet states of bare VS^+ and assuming that the contribution of the CS unit to the SOC is negligible. These calculations yield a coupling constant of ~ 20 cm^{-1} (0.0025 eV) as the average over all possible spin–orbit states of diatomic VS^+. Thus, the spin–orbit coupling lies in the weak-coupling limit.[42]

In the subsequent discussion, we therefore consider that the spin-forbidden reaction (5) is strongly influenced by interaction of the two adiabatic potential-energy surfaces at the MECP. However, the calculated potential-energy surface may allow for an alternative mechanism. Specifically, bond activation in the $[V,C,S_2]^+$ system may proceed entirely on the quintet surface to form $SV(CS)^+(^5A'')$, and spin inversion to the triplet surface occurs via coupling of the rovibrational modes of the ground and excited $SV(CS)^+$ states. Such a process is referred to as intersystem crossing (ISC), i.e., conversion of electronic into rovibrational energy.[39] ISC seems conceivable in light of the similar geometries of $\mathbf{2}(^3A'')$ and $\mathbf{2}(^5A'')$, which primarily differ in r_{V-S}, such that the V–S stretch may allow for coupling of the two surfaces. In the gas phase, ISC is usually considered to be important only for molecules much larger than $[V,C,S_2]^+$. Further, the significant energy gap between $SV(CS)^+(^3A'')$ and $SV(CS)^+(^5A'')$ implies that the triplet ground state would be formed in a high vibrational level, i.e., $v\approx 15$ on the basis of a calculated harmonic V–S stretch of 537 cm^{-1} in $SV(CS)^+(^3A'')$. This large change in the vibrational quantum number is likely to significantly reduce the overlap of the respective wave functions. For the time being, we cannot assess this aspect more accurately due to the lack of an appropriate formalism to describe ISC in $[V,C,S_2]^+$.

Several models have been developed to quantitatively describe the probability of surface crossings. In the limit of a one-dimensional potential-energy surface, the crossing probability can be described by the Landau–Zener (LZ) model,[40]

$$P_{LZ}=\exp\{-[c/(E-E_c)]^{1/2}\}. \tag{11}$$

In Eq. (11), P_{LZ} is the probability of crossing between adiabatic potential-energy surfaces during a single pass through the avoided crossing region, c is a surface coupling term that depends on the energy gap between the adiabatic curves ($2H_{SO}$) and inversely on the difference in the slopes of the diabatic curves at the crossing point, E is the relative kinetic energy of the reactants, and E_c is the potential energy of the crossing point. As discussed in the Appendix, the total LZ probability for forming a spin-forbidden product, p_N, is dependent on the number of passes, N, the system makes through the intersection region. Nevertheless, the energy dependences of p_1, p_2, and P_∞ are all approximately $[c/(E-E_c)]^{1/2}$ in the weak-coupling limit of small c (see the Appendix).

In the Landau–Zener model, the single dimension refers to the relative translational motion of the reactants. For multidimensional surfaces, it is possible that the component of the nuclear velocity perpendicular to the surface-crossing seam, which determines the crossing probability,[41–43] is more like a vibration than a translation. *A priori*, we cannot deduce whether the crossing mechanism is primarily dependent on the translational or vibrational motion of the system, but this determination is unnecessary for our threshold analysis. For example, vibrationally coupled, spin-forbidden charge-transfer reactions can also exhibit $E^{-1/2}$ energy dependencies.[44] Further, in a statistical limit, it has been shown that the crossing probability between diabatic surfaces of different spin multiplicities has an $(E-E_c)^{-1/2}$ dependence for weakly coupled diabatic surfaces regardless of the dimensionality of the hypersurface, where E is the total energy available to the system.[43,45,46] In the present experiments, E is essentially the translational energy of the reactants. Thus the $(E-E_c)^{-1/2}$ energy dependence is a general approximation to the surface-crossing behavior that is appropriate for a variety of crossing mechanisms.

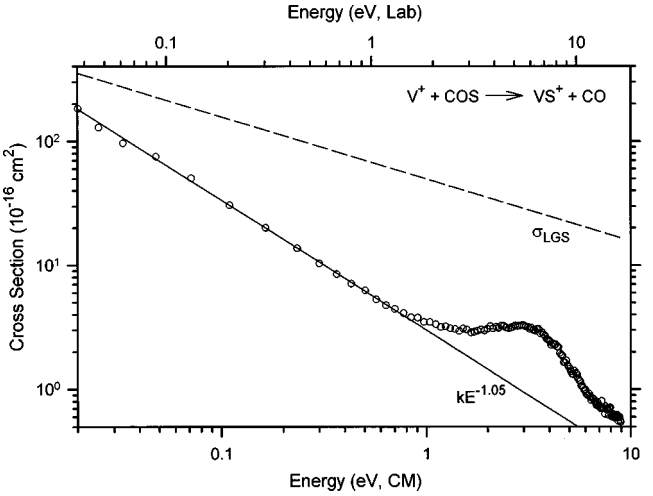

FIG. 6. Cross section for VS^+ formation (○) in reaction (12) as a function of kinetic energy in the center-of-mass (lower axis) and laboratory (upper axis) frames. The Langevin–Gioumousis–Stevenson (LGS) cross section (the broken line) declines as $E^{-0.5}$, while the exothermic VS^+ cross section declines approximately as E^{-1} (the solid line).

Some experimental confirmation of the simple $(E-E_c)^{-1/2}$ energy dependence for surface crossing in the present system comes from recent studies of reaction (12),[26] which is isoelectronic with reaction (1),

$$V^+ + COS \rightarrow VS^+ + CO. \tag{12}$$

Results for this exothermic process are shown in Fig. 6. Cross sections for exothermic ion–molecule reactions typically decline with an energy dependence proportional to $E^{-1/2}$, as predicted by the Langevin–Gioumousis–Stevenson (LGS) model[47] for collisions between ions and polarizable molecules:

$$\sigma_{LGS}(E)=\pi e(2\alpha/E)^{1/2}, \tag{13}$$

where α is the polarizability of the neutral molecule and e is the electron charge. The energy dependence of the exothermic feature associated with reaction (12), however, declines

approximately as E^{-1}. This appears to represent the combined effect of both the surface crossing and LGS behaviors (in the limit that $E>E_c$).

To incorporate this surface-crossing energy dependence into our threshold analysis of reaction (5), we multiply Eq. (3) by $E^{-1/2}$,

$$\sigma(E)_{LZ}=E^{-1/2}\cdot\sigma(E), \tag{14}$$

which is equivalent to using Eq. (3) with $m=1.5$. This approach is particularly convenient and flexible, because adjustments to n during optimization can compensate for small errors introduced by the $E^{-1/2}$ approximation to the actual crossing behavior. $E^{-1/2}$ is used instead of $(E-E_c)^{-1/2}$ (derived from statistical considerations[43,45]) or p_N (derived in the Appendix) because E_c and c are uncertain.

To determine whether the $E^{-1/2}\cdot\sigma(E)$ approximation provides a reliable estimate of the threshold of a cross section having the form $p_n\cdot\sigma(E)$, we simulated experimental cross sections by calculating 36 different $p_N\cdot\sigma(E)$ test cross sections.[48] The p_1, p_2, and p_∞ functions used c values ranging from 0.001 to 1 eV and E_c values from -0.6 to 1.0 eV. The arbitrary trial function of $\sigma(E)=(E-E_0)^n/E$ used $E_0=0.78$ eV and $n=0.5$. We then convoluted the test curves with typical GIB experimental conditions to yield $\mathbf{C}[p_N\cdot\sigma(E)]$ test curves, where $\mathbf{C}$ is the convolution operator. These convoluted test curves were then modeled using Eq. (3) with $m=1.5$ and an average threshold of 0.77 ± 0.01 eV was obtained. We also examined the effect of different n values (0.25 and 1.0) for the trial function and observed equally good results (deviations less than 0.01 eV from the trial E_0 value). Therefore, as long as the spin-forbidden process exhibits a power-law energy dependence, the empirical modeling appears to be capable of providing a reliable estimate of the energy threshold, certainly within any typical experimental error. For convenience, threshold analyses using Eq. (14) are subsequently referred to as LZ analyses, even though our approach is not uniquely based on the Landau–Zener model.

E. Landau–Zener analysis of the VS^+ cross section

Extensive LZ analyses of the first feature in the quintet VS^+ cross sections of several data sets (SI and DC/FT) using Eq. (14) with $\sigma_0(^5F)/\sigma_0(^5D)$ reactivity ratios from 0 to 1.0 reproduce the data well with $\sigma_0(^5F)/\sigma_0(^5D)=0.75\pm0.25$. A typical LZ fit to the DC/FT (cooled) data is shown in Fig. 7. Note that the convoluted fit obtained using Eq. (14) is able to reproduce both the threshold region and the decline of the first feature because it incorporates the $E^{-1/2}$ surface-crossing probability. By contrast, only the threshold region below 1 eV can be modeled using Eq. (3); the decline at higher energies is not faithfully reproduced.

Table IV compares the fitting parameters obtained in the LZ analysis using Eq. (14) ($m=1.5$) with those obtained using Eq. (3) ($m=1.0$), and shows that the values of σ_0, E_0, and n obtained from the two models are the same within experimental uncertainty. Both models yield $n\approx0.5$, the theoretical value of n derived from microscopic reversibility arguments for endothermic ion–molecule reactions.[49] Based on these results, we conclude that the decline of the first feature is governed by the energy dependence of the surface-crossing step in the spin-forbidden reaction (5), and that the $E^{-1/2}$ approximation is adequate to quantitatively describe the energy dependence of the adiabatic behavior in this system.

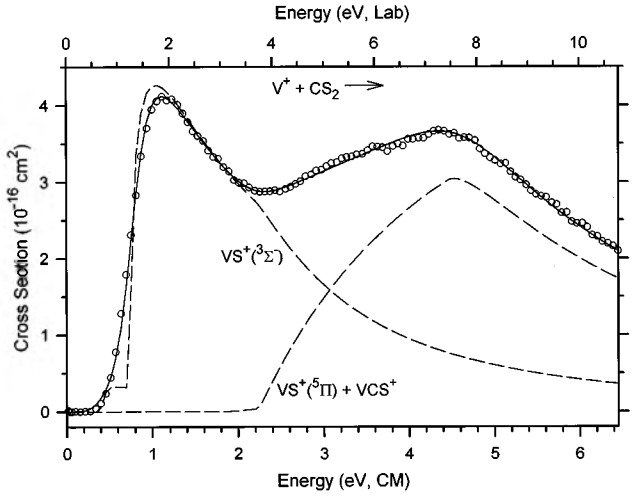

FIG. 7. Total cross section (○) for reactions (1) and (2) as a function kinetic energy in the center-of-mass (lower axis) and laboratory (upper axis) frames. The estimated 0 K cross sections for formation of $VS^+(^3\Sigma^-)$ and the sum of $VS^+(^5\Pi)+[V,C,S]^+$ are shown by the broken lines. The full line shows the sum of these after convolution over the experimental energy distributions.

Different values of m, ranging from 1.0 to 2.0, were used to examine the possibility that the adiabatic behavior has an energy dependence other than $E^{-1/2}$. The measured thresholds are not very sensitive to these changes (within 0.01 eV), though the optimized values of n vary substantially (from 0.25 to 0.65) to compensate for the different m values. The best fits to the data are obtained with $m=1.5$, and the fits grow progressively poorer as m deviates from 1.5. This is an experimental confirmation of the $E^{-1/2}$ power-law dependence for the spin-forbidden process.

Our extensive analysis of the threshold region of the VS^+ cross section with different models and different $\sigma_0(^5F)/\sigma_0(^5D)$ reactivity ratios leads to a conservative estimate of the threshold for reaction (5) of 0.78 ± 0.08 eV. From this threshold, we calculate $D_0(V^+-S)=3.72\pm0.09$ eV, in good agreement with $D_0(V^+-S)=3.78\pm0.10$ eV derived in a comprehensive experimental and theoretical study of VS^+ thermochemistry.[26] The agreement between these values also implies that the spin-forbidden formation of ground state $VS^+(^3\Sigma^-)$ from ground state $V^+(^5D)$ does not have a barrier in excess of the reaction

TABLE IV. Summary of fitting parameters for the $V^+ + CS_2$ reactions.

Products	Model Eq.	σ_0	E_0	n
$VS^+(^3\Sigma^-)+CS^a$	3 ($m=1$)	7.1 (1.4)	0.75 (0.05)	0.52 (0.12)
$VS^+(^3\Sigma^-)+CS$	14 ($m=1.5$)	7.6 (1.1)	0.81 (0.04)	0.48 (0.06)
$VS^+(^5\Pi)+CS$	3,4 ($m=1$)	5.6 (1.6)	2.23 (0.14)	1.2 (0.2)
$V(CS)^+ + S$	3,4 ($m=1$)	1.9 (0.4)	2.80 (0.07)	1.8 (0.2)
$CVS^+ + S$	3 ($m=1$)	1.6 (0.7)	5.60 (0.20)	0.84 (0.07)

[a]Average of values in the bottom half of Table II.

endothermicity. In other words, the intersection of the diabatic ground state reactant and product potential-energy surfaces lies well below the product asymptote. This conclusion coincides with the theoretically predicted surfaces shown in Fig. 5.

By subtracting a fit of the first feature due to reaction (5) from the experimental VS^+ cross section, one can estimate the shape of the second feature associated with the spin-allowed reaction (6). This procedure is problematic because the high-energy (above 2 eV) behavior of reaction (5) is unknown and the competitive formation of the $[V,C,S]^+$ product further perturbs the energy dependence of the VS^+ cross section. Both factors complicate the modeling of the second feature. To overcome these problems, we first make the reasonable assumption that process (5) is attenuated to some degree by competition with reaction (6) and examine several possibilities for the high-energy behavior of reaction (5). We then subtract these estimates from the total cross section, rather than the VS^+ cross section, which is equivalent to estimating the shape of the cross section for reaction (6) in the absence of competition from the $[V,C,S]^+$ channel. The resulting cross sections for reaction (6) are then analyzed with Eq. (3) ($m=1$). An example of this type of analysis is shown in Fig. 7. We find that the threshold determined for the second feature is not very sensitive to variations in the assumed high-energy behavior of reaction (5). The average values of σ_0, E_0, and n obtained from several acceptable fits of the second feature are given in Table IV.

Combining these results, we estimate the adiabatic excitation energy from the $VS^+(^3\Sigma^-)$ ground state to the $VS^+(^5\Pi)$ excited state as the energy difference between the thresholds of the first (0.78 ± 0.08 eV) and second features (2.23 ± 0.14 eV) in the VS^+ cross section. This value, 1.45 ± 0.16 eV, is in good agreement with the theoretically calculated value of 1.37 eV.[26]

F. Analysis of the $[V,C,S]^+$ channel

As mentioned above, the experimentally observed $[V,C,S]^+$ cross section shown in Fig. 3 is believed to be a composite of two features, attributable to the formation of $V(CS)^+$ in reaction (2) and to formation of either an excited state of $V(CS)^+$ or to the CVS^+ isomer according to reaction (8), respectively. Analysis of the lowest-energy region of the $[V,C,S]^+$ cross section with Eq. (4) yields an average threshold of 2.80 ± 0.07 eV which we attribute to the formation of the thiocarbonyl complex $V(CS)^+$. The optimized fitting parameters are given in Table IV and the reproduction of the data is shown in Fig. 8. From this threshold and $D_0(SC-S)=4.50\pm0.04$ eV, we calculate $D_0(V^+-CS)=1.70\pm0.08$ eV. Preliminary B3LYP/6-311+G* calculations predict a quintet ground state of $V(CS)^+(^5\Delta)$ with $D_0(V^+-CS)=1.44$ eV. The use of Eq. (4) allows us to model the decline in this cross section due to dissociation of the $V(CS)^+$ product to $V^+ + CS$ starting at 4.5 eV. Such a model is somewhat speculative because there is only a very narrow energy region over which this cross section declines. Nevertheless, by subtracting this model from the $[V,C,S]^+$ cross section, we can estimate the cross section for the second process that appears to contribute at higher energies. Analysis of the high-energy portion of the $[V,C,S]^+$ cross section with Eq. (3) yields an approximate threshold of 5.6 ± 0.2 eV. Figure 8 shows that the composite of these two cross sections reproduces the data in detail over an extended range of energies.

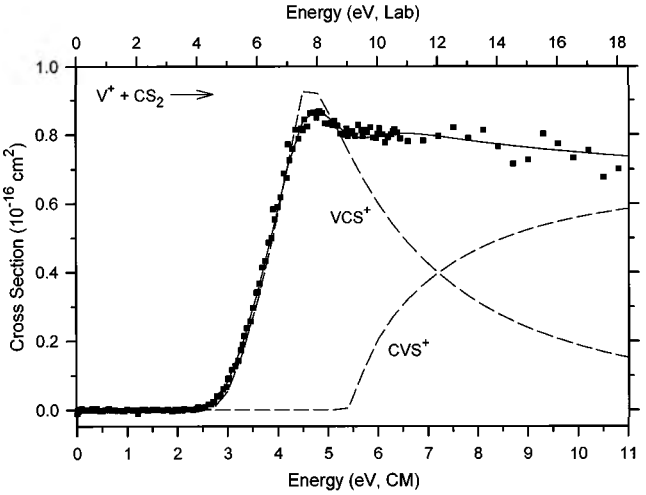

FIG. 8. Cross section for $[V,C,S]^+$ formation (■) in reaction (2) as a function of kinetic energy in the center-of-mass (lower axis) and laboratory (upper axis) frames. The estimated 0 K cross sections for formation of $V(CS)^+$ and CVS^+ are shown by the broken lines. The full line shows the sum of these after convolution over the experimental energy distributions.

This thermochemistry can now be used to analyze the high energy portion of the $[V,C,S]^+$ channel in more detail. The energy difference between the two experimentally observed processes, 2.8 ± 0.2 eV, is inconsistent with the theoretically determined excitation energy of 0.81 eV from the $V(CS)^+(^5\Delta)$ to the $V(CS)^+(^3\Phi)$ excited state or the known excitation energy of 1.15 eV for the $S(^3P)-S(^1D)$ splitting.[50] We are tempted to attribute the second process to the formation of CVS^+ in reaction (8), but preliminary calculations suggest that the structure of the high energy isomer could either be inserted CVS^+ or a side-on coordinated CS ligand.[51]

IV. SUMMARY AND CONCLUSIONS

The kinetic-energy dependence of the $V^+ + CS_2$ reaction is examined using guided ion beam mass spectrometry. Different ion sources are used to systematically vary the electronic state distribution of the V^+ reactant. Compared to the $V^+(^5D)$ ground state, the $V^+(^5F)$ first excited state is found to be about $75\pm25\%$ as reactive toward CS_2.

The cross section for VS^+ formation exhibits distinct endothermic features corresponding to the spin-forbidden formation of ground state $VS^+(^3\Sigma^-)$ and the spin-allowed formation of excited state $VS^+(^5\Pi)$. The difference in the thresholds of these two features, 1.45 ± 0.16 eV, is in good agreement with the theoretically predicted excitation energy between the $VS^+(^3\Sigma^-)$ and $VS^+(^5\Pi)$ states of 1.37 eV.[26] Because the formation of the $VS^+(^3\Sigma^-)$ ground state requires a spin inversion, this process is an example of two-state reactivity. An $E^{-1/2}$ approximation appears to be adequate to quantitatively describe the kinetic-energy

dependence of the adiabatic behavior in this system and agrees nicely with theoretical predictions.[43,45,46]

The kinetic-energy dependence of the $[V,C,S]^+$ product implies that ground state $V(CS)^+$ and probably a high-energy isomer are formed. This suggests that the activation of the CS_2 molecule by V^+ proceeds through an inserted $S–V^+–C–S$ intermediate. An analysis of the features in the $[V,C,S]^+$ cross section leads to $D_0(V^+–CS)=1.70 \pm 0.08$ eV for the thiocarbonyl complex $V(CS)^+$.

ACKNOWLEDGMENTS

This work is supported by the National Science Foundation. The Berlin group acknowledges support by the Deutsche Forschungsgemeinschaft, the Volkswagen-Stiftung, and the Fonds der Chemischen Industrie.

APPENDIX: LANDAU–ZENER SURFACE-CROSSING PROBABILITY FOR MULTIPLE TRAVERSALS

In the LZ model, the total probability for forming a spin-forbidden product, p_N, is dependent on the number of passes, N, the system makes through the intersection region. For a single traversal of the intersection region this is given by Eq. (A1), where P is the crossing probability according to the Landau–Zener model,

$$p_1=1-P. \tag{A1}$$

For atomic reactants, two traversals must occur (one as the reactants approach and a second as they separate). For spin inversion to occur in this case, the system must behave adiabatically during the approach and diabatically during the exit, or vice-versa. Thus, the net probability for a spin-forbidden event is the product of the adiabatic and diabatic traversal probabilities,

$$p_2=2P(1-P). \tag{A2}$$

The factor of 2 accounts for the fact that the adiabatic traversal may occur either during the approach or the exit. For multidimensional potential-energy surfaces such as those appropriate for the $[V,C,S_2]^+$ system, more traversals may be possible. The calculated potential-energy curves for the $[V,C,S_2]^+$ system are shown in Fig. 5. In the discussion that follows, we consider only transitions between these diabatic ground state surfaces.

As the reaction energy increases to the threshold energy for VS^+ formation, a fraction of the system's population, $1-P$, follows the adiabatic pathway to products, while the remaining fraction, P, continues to move upwards to position **A** on the diabatic quintet surface. The fraction that proceeds to products is effectively removed from consideration, while the fraction at position **A** remains active and will traverse the intersection again on the way down. At the intersection, the active fraction is again divided, with $(P)^2$ of the original population returning to reactants and $P(1-P)$ of the original population crossing to position **B** on the diabatic triplet surface. Clearly, the active population will continue to oscillate between points **A** and **B**, and with each traversal more and more of the population eventually finds its way out the entrance or exit channels. The total fraction of the original population that goes on to products, p_∞, is given by an infinite sum:

$$p_\infty=1-P+P^2(1-P)+P^2(1-P)^3+P^2(1-P)^5+\ldots. \tag{A3}$$

The total fraction that returns to reactants is given by

$$1-p_\infty=P^2+P^2(1-P)^2+P^2(1-P)^4+P^2(1-P)^6+\ldots. \tag{A4}$$

These quantities can be expressed in closed form as:

$$p_\infty=(1-P)[2/(2-P)], \tag{A5}$$

$$1-p_\infty=P/(2-P). \tag{A6}$$

As the reaction energy increases to the energy of the $VS^+(^5\Pi)+CS$ exit channel, the probability for multiple traversals reduces. In the limit of a one-dimensional surface, the total probability for forming products at these energies is simply $p_1=1-P$. Of course, this simplistic approach ignores the possibility of other surface crossings, as well as other dimensions on the $[V,C,S_2]^+$ hypersurface. Nevertheless, it is interesting to note that p_1, p_2, and p_∞, which represent the limits of the possible behavior of the system, all approach an $(E-E_c)^{-1/2}$ energy dependence at higher kinetic energies. This is most easily seen by noting that p_1, p_2, and p_∞ contain the term $(1-P)$, which is approximately $[c/(E-E_c)]^{1/2}$ in the weak coupling limit (small c). At higher energies, P approaches unity such that Eqs. (A1), (A2), and (A5) have energy dependencies of $[c/(E-E_c)]^{1/2}$. This conclusion, derived from a rather simplistic description of the potential-energy surface, is in agreement with the results of more sophisticated models.[43,45]

To illustrate the energy dependence of the LZ surface-crossing probability, p_1 and p_∞ are plotted as a function of the reactant kinetic energy in Fig. 9 for a case where $c=0.05$ eV. Note that the probability of a net surface tran-

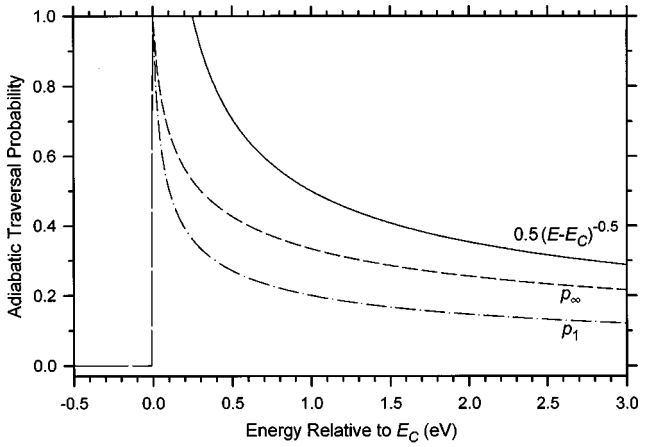

FIG. 9. Adiabatic behavior probabilities predicted by the Landau–Zener model as a function of kinetic energy relative to E_c for a single pass through the surface intersection (p_1) and for an infinite number of passes (p_∞). For both curves, $c=0.05$ eV. The function, $0.5(E-E_c)^{-0.5}$, is also shown for comparison.

sition has a maximum when the reactant kinetic energy is close to the potential energy of the crossing barrier E_c, i.e., when the reactants pass slowly through the crossing region. Above E_c, p_1 and p_∞ decline approximately as $(E-E_c)^{-1/2}$, which is approximated by $E^{-1/2}$ when $E>E_c$. This appears to be an adequate first approximation of the adiabatic behavior in the $[V,C,S_2]^+$ system.

[1] P. B. Armentrout, Annu. Rev. Phys. Chem. **41**, 313 (1990).
[2] P. B. Armentrout, Science **251**, 175 (1991).
[3] A. Fiedler, D. Schröder, H. Schwarz, and S. Shaik, J. Am. Chem. Soc. **116**, 10734 (1994); S. Shaik, D. Danovich, A. Fiedler, D. Schröder, and H. Schwarz, Helv. Chim Acta **78**, 1393 (1995); A. Fiedler, D. Schröder, W. Zummack, and H. Schwarz, Inorg. Chim. Acta **259**, 227 (1997); S. Shaik, M. Filatov, D. Schröder, and H. Schwarz, Chem.-Eur. J. **4**, 193 (1998).
[4] D. A. Plattner, Angew. Chem. **111**, 86 (1999); Angew. Chem. Int. Ed. Engl. **38**, 82 (1999).
[5] G. F. Stowe, R. H. Schultz, C. A. Wight, and P. B. Armentrout, Int. J. Mass Spectrom. Ion Processes **100**, 177 (1990).
[6] R. H. Schultz, J. L. Elkind, and P. B. Armentrout, J. Am. Chem. Soc. **110**, 411 (1988); D. E. Clemmer, Y.-M. Chen, F. A. Khan, and P. B. Armentrout, J. Phys. Chem. **98**, 6522 (1994); D. Schröder, H. Schwarz, D. E. Clemmer, Y.-M. Chen, P. B. Armentrout, V. I. Baranov, and D. K. Bohme, Int. J. Mass Spectrom. Ion Processes **161**, 175 (1997); P. A. M. van Koppen, M. T. Bowers, C. L. Haynes, and P. B. Armentrout, J. Am. Chem. Soc. **120**, 5704 (1998).
[7] K. M. Ervin and P. B. Armentrout, J. Chem. Phys. **83**, 166 (1985).
[8] R. H. Schultz and P. B. Armentrout, Int. J. Mass Spectrom. Ion Processes **107**, 29 (1991).
[9] E. Teloy and D. Gerlich, Chem. Phys. **4**, 417 (1974); D. Gerlich, Adv. Chem. Phys. **82**, 1 (1992).
[10] R. A. McDonald and A. N. Syverud, J. Phys. Chem. Ref. Data **14**, Suppl. 1 (JANAF TABLES) (1985).
[11] M. E. Weber, J. L. Elkind, and P. B. Armentrout, J. Chem. Phys. **84**, 1521 (1986).
[12] E. R. Fisher, B. L. Kickel, and P. B. Armentrout, J. Chem. Phys. **97**, 4859 (1992); C. L. Haynes and P. B. Armentrout, Organometallics **13**, 3480 (1994); F. A. Khan, D. L. Steele, and P. B. Armentrout, J. Phys. Chem. **99**, 7819 (1995); Y.-M. Chen and P. B. Armentrout, J. Chem. Phys. **103**, 618 (1995).
[13] N. Aristov and P. B. Armentrout, J. Phys. Chem. **91**, 6178 (1987).
[14] These processes will not occur in the flow tube, because formation of VCH_2^+ and VO^+ from reaction of $V^+(^5F)$ with CH_4 and NO is endothermic by 0.44 and 0.18 eV, respectively; see: P. B. Armentrout and B. L. Kickel, in *Organometallic Ion Chemistry*, edited by B. S. Freiser (Kluwer: Dordrecht, 1996), pp. 1–45.
[15] L. S. Sunderlin and P. B. Armentrout, J. Phys. Chem. **92**, 1209 (1988).
[16] R. H. Garstang, Mon. Not. R. Astron. Soc. **124**, 321 (1962). R. H. Garstang (personal communication).
[17] P. R. Kemper and M. T. Bowers, J. Phys. Chem. **95**, 5134 (1991).
[18] J. L. Elkind and P. B. Armentrout, J. Phys. Chem. **89**, 5626 (1985).
[19] A. D. Becke, J. Chem. Phys. **98**, 5648 (1993).
[20] C. Lee, W. Yang, and R. G. Parr, Phys. Rev. B **37**, 785 (1988); B. Miehlich, A. Savin, H. Stoll, and H. Preuss, Chem. Phys. Lett. **157**, 200 (1989).
[21] M. J. Frisch, G. W. Trucks, H. B. Schlegel, P. M. W. Gill, B. G. Johnson, M. A. Robb, J. R. Cheeseman, T. Keith, G. A. Petersson, J. A. Montgomery, K. Ragavachari, M. A. Al-Laham, V. G. Zakrezewski, J. V. Oritz, J. B. Foresman, C. Y. Peng, P. Y. Ayala, W. Chen, M. W. Wong, J. L. Andres, E. S. Replogle, R. Gomperts, R. L. Martin, D. J. Fox, J. S. Binkley, D. J. DeFrees, J. Baker, J. J. P. Stewart, M. Head-Gordon, C. Gonzales, and J. A. Pople, GAUSSIAN Inc., Pittsburgh, PA, 1995.
[22] M. W. Schmidt, *et al.* J. Comput. Chem. **14**, 1347 (1993). The version for personal computers was compiled by A. A. Granovsky, Moscow State University.
[23] M. S. Gordon, Chem. Phys. Lett. **76**, 163 (1980).
[24] A. J. H. Wachters, J. Chem. Phys. **52**, 1033 (1970).
[25] S. Koseki, M. W. Schmidt, and M. S. Gordon, J. Phys. Chem. **96**, 10768 (1992); S. Koseki, M. S. Gordon, M. W. Schmidt, and N. Matsunaga, *ibid.* **99**, 12764 (1995).
[26] I. Kretzschmar, D. Schröder, H. Schwarz, C. Rue, and P. B. Armentrout, J. Phys. Chem. A **102**, 10060 (1998).
[27] J. L. Elkind and P. B. Armentrout, J. Phys. Chem. **90**, 6576 (1986).
[28] For an impressive example of this statement, see: J. V. B. Oriedo and D. H. Russell, J. Am. Chem. Soc. **115**, 8376 (1993).
[29] It is also possible that the CS_2 reactant contains a very small amount (0.03%) of OCS, which reacts with V^+ at thermal energies to form VS^+.
[30] B. L. Kickel and P. B. Armentrout, J. Am. Chem. Soc. **117**, 764 (1995); Y.-M. Chen, J. L. Elkind, and P. B. Armentrout, J. Phys. Chem. **99**, 10438 (1995).
[31] J. Sugar and C. Corliss, J. Phys. Chem. Ref. Data **14**, Suppl. 2 (1985).
[32] This is the state separation properly averaged over the spin–orbit levels. The uncertainty refers to the range of values obtained for source temperatures appropriate for this study (1250–2300 K).
[33] L. Sanders, S. D. Hanton, and J. C. Weisshaar, J. Chem. Phys. **92**, 3498 (1990).
[34] K. J. Miller, J. Am. Chem. Soc. **112**, 8533 (1990).
[35] G. Herzberg, *Molecular Spectra and Molecular Structure*, 2nd ed. (Van Nostrand, New York, 1950), Vol. I.
[36] M. R. Sievers and P. B. Armentrout, J. Chem. Phys. **102**, 754 (1995).
[37] For a simple method to locate MECPs, see: J. N. Harvey, M. Aschi, H. Schwarz, and W. Koch, Theor. Chem. Acc. **99**, 95 (1998). See also: M. Aschi, J. N. Harvey, C. A. Schalley, D. Schröder, and H. Schwarz, J. Chem. Soc. Chem. Commun. **1998**, 531.
[38] For estimation of the crossing probability, see: S. A. Mitchell, in *Gas Phase Metal Reactions*, edited by A. Fontijn (North-Holland, Amsterdam, 1992), p. 227; D. Schröder, C. Heinemann, H. Schwarz, J. N. Harvey, S. Dua, S. J. Blanksby, and J. H. Bowie, Chem. Eur. J. **4**, 2550 (1998).
[39] M. Klessinger and J. Michl, *Lichtabsorption und Photochemie organischer Moleküle* (VCH, Weinheim, 1989).
[40] T. Baer and W. L. Hase, *Unimolecular Reaction Dynamics* (Oxford University Press, New York, 1996), p. 316, and references therein.
[41] J. C. Tully, *Dynamics of Molecular Collisions*, edited by W. H. Miller (Plenum, New York, 1976), Part B.
[42] G. E. Zahr, R. K. Preston, and W. H. Miller, J. Chem. Phys. **62**, 1127 (1975).
[43] E. J. Heller and R. C. Brown, J. Chem. Phys. **79**, 3336 (1983).
[44] R. A. Dressler, S. T. Arnold, and E. Murad, J. Chem. Phys. **103**, 9989 (1995).
[45] J. C. Lorquet and B. Leyh-Nihant, J. Phys. Chem. **92**, 4778 (1988).
[46] References 43 and 45 derive expressions for rate constants. The energy dependence of the surface-crossing probability is most easily obtained from Eq. (4.12) in Ref. 45, ignoring the zero-point energy terms in the semiclassical density of states expressions. P can be given as $(E-E_c)^{u-1/2}/(E)^u$ where u is the number of degrees of freedom excluding the coordinate perpendicular to the surface-crossing seam.
[47] G. Gioumousis and D. P. Stevenson, J. Chem. Phys. **29**, 294 (1958).
[48] Results for the various test curves are available from the authors upon request.
[49] P. B. Armentrout, in *Advances in Gas Phase Ion Chemistry*, edited by N. G. Adams and L. M. Babcock (JAI, Greenwich, 1992), Vol. 1, p. 83; K. M. Ervin and P. B. Armentrout, J. Chem. Phys. **80**, 2978 (1984).
[50] C. E. Moore, Atomic Energy Levels, NSRDS-NBS 35 (1971).
[51] Relative energies of the located minima at the B3LYP/6-311+G* level with respect to the $^5\Delta$ ground state of $V(CS)^+$ for CVS^+ inserted structures are 6.01 eV for $^5\Sigma$ and 3.56 eV for $^3A'$ and for a side-on structure is 1.69 eV for $^1A'$.